A Novel Pyrazolo[3,4-*d*]pyrimidine Induces Heme Oxygenase-1 and Exerts Anti-Inflammatory and Neuroprotective Effects

Ji Ae Lee[1], Young-Won Kwon[1], Hye Ri Kim[1], Nari Shin[1], Hyo Jin Son[1], Chan Seong Cheong[2], Dong Jin Kim[2,*], and Onyou Hwang[1,*]

[1]Department of Biochemistry and Molecular Biology, University of Ulsan College of Medicine, Seoul 05505, Korea, [2]Center for Neuro-Medicine, Brain Science Institute, Korea Institute of Science and Technology, Seoul 02792, Korea
*Correspondence: oyhwang@amc.seoul.kr (OH); djk2991@kist.re.kr (DJK)
https://doi.org/10.14348/molcells.2021.0074
www.molcells.org

The anti-oxidant enzyme heme oxygenase-1 (HO-1) is known to exert anti-inflammatory effects. From a library of pyrazolo[3,4-*d*]pyrimidines, we identified a novel compound KKC080096 that upregulated HO-1 at the mRNA and protein levels in microglial BV-2 cells. KKC080096 exhibited anti-inflammatory effects via suppressing nitric oxide, interleukin-1β (IL-1β), and iNOS production in lipopolysaccharide (LPS)-challenged cells. It inhibited the phosphorylation of IKK and MAP kinases (p38, JNK, ERK), which trigger inflammatory signaling, and whose activities are inhibited by HO-1. Further, KKC080096 upregulated anti-inflammatory marker (Arg1, YM1, CD206, IL-10, transforming growth factor-β [TGF-β]) expression. In 1-methyl-4-phenyl-1,2,3,6-tetrahydropyridine-treated mice, KKC080096 lowered microglial activation, protected the nigral dopaminergic neurons, and nigral damage-associated motor deficits. Next, we elucidated the mechanisms by which KKC080096 upregulated HO-1. KKC080096 induced the phosphorylation of AMPK and its known upstream kinases LKB1 and CaMKKbeta, and pharmacological inhibition of AMPK activity reduced the effects of KKC080096 on HO-1 expression and LPS-induced NO generation, suggesting that KKC080096-induced HO-1 upregulation involves LKB1/AMPK and CaMKKbeta/AMPK pathway activation. Further, KKC080096 caused an increase in cellular Nrf2 level, bound to Keap1 (Nrf2 inhibitor protein) with high affinity, and blocked Keap1-Nrf2 interaction. This Nrf2 activation resulted in concurrent induction of HO-1 and other Nrf2-targeted antioxidant enzymes in BV-2 and in dopaminergic CATH.a cells. These results indicate that KKC080096 is a potential therapeutic for oxidative stress- and inflammation-related neurodegenerative disorders such as Parkinson's disease.

Keywords: heme oxygenase-1, neuroinflammation, Parkinson's disease, pyrazolo[3,4-*d*]pyrimidine

INTRODUCTION

Neuroinflammation is known to play a critical role in the pathogenesis of neurodegenerative disorders including Parkinson's disease (PD). It is caused by the activation of microglia, the brain's resident immune cells. While these cells serve a role as part of the injury response, their chronic or excessive activation causes neurotoxic degeneration of the nearby neurons, thereby contributing to PD pathogenesis. The current therapeutic interventions are aimed at mitigating the symptoms alone, thus making it essential to develop therapeutic strategies that can prevent or delay the disease progression.

Recent studies have demonstrated that the enzyme

heme oxygenase-1 (HO-1) can suppress inflammation. Its activity has been associated with the shift from the M1-like proinflammatory microglial phenotype to the M2-like anti-inflammatory phenotype (Naito et al., 2014; Sierra-Filardi et al., 2010; Tu et al., 2014). This anti-inflammatory effect is thought to be mediated via the modulation of inflammatory signaling, which involves IκB kinase (IKK) leading to NFκB activation (Kawai and Akira, 2007) and the MAP kinases ERK, JNK, and p38 MAPK (Arthur and Ley, 2013). HO-1 has been shown to inhibit the IKK/IκB/NFκB and MAP kinase pathways (Li et al., 2008; Morse et al., 2003; Silva et al., 2006).

HO-1 expression is controlled by the transcription factor Nrf2 (Alam et al., 1999). As expected, the absence of Nrf2/HO-1 leads to reduced anti-inflammatory activity (Poss and Tonegawa, 1997; Rojo et al., 2014; Wiesel et al., 2000). The expression of HO-1 can also be increased by the enzyme AMP kinase (AMPK) (Al-Rashed et al., 2018; Thornton et al., 2016), and AMPK inhibition suppresses HO-1 induction and its ability to prevent inflammation (Al-Rashed et al., 2018). Hence, agents that lead to the activation of Nrf2/HO-1 and AMPK/HO-1 pathways can be of translational value.

Pyrazolopyrimidines are fused heterocyclic ring systems. Among these, the pyrazolo[3,4-*d*]pyrimidines have been noted for their various biological activities and are thought to be therapeutically significant (Chauhan and Kumar, 2013). Here, we introduce a novel pyrazolo[3,4-*d*]pyrimidine KKC080096 that activates both Nrf2 and AMPK signaling pathways, leading to HO-1 upregulation. The compound exhibits anti-inflammatory properties, is neuroprotective, and prevents the motor deficits in a PD animal model, thereby demonstrating a therapeutic potential for neurodegenerative diseases.

MATERIALS AND METHODS

Materials

Dulbecco's modified Eagle's medium (DMEM), RPMI 1640, horse serum, fetal bovine serum (FBS), trypsin/EDTA, penicillin-streptomycin, and streptavidin-agarose beads were obtained from Thermo Fisher Scientific (USA). 1-Methyl-4-phenyl-1,2,3,6-tetrahydropyridine (MPTP), Compound C, adenine 9-β-D-arabinofuranoside (Ara A), and lipopolysaccharide (LPS) were purchased from Sigma-Aldrich (USA). Sulfanilamide and naphthylethylenediamine dihydrochloride were procured from Fluka Chemika-Biochemika (Switzerland), and the Bradford assay kit was from Bio-Rad (UK). First strand cDNA synthesis kit for reverse transcription polymerase chain reaction (RT-PCR) was purchased from MBI Fermentas (Canada). The following primary antibodies were used: anti-iNOS (sc-650), anti-HO-1 (sc-10789), anti-Nrf2 (sc-30915), anti-glutamate-cysteine ligase modifier subunit (GCLM) (sc-22754), anti-DJ-1 (sc-27004), lamin B (sc-6216), and anti-IKK (sc-7607) (all from Santa Cruz Biotechnology, USA); anti-glutamate-cysteine ligase catalytic subunit (GCLC; Novus Biologicals, USA) (NBP1-49762); anti-Iba-1 (SAN3725) (Wako Chemicals, Japan); anti-HSP90 (#4877), anti-p-IKK (#2697), anti-ERK (#9102), anti-p-ERK (#9101), anti-p38 (#9212), anti-p-p38 (#9211), anti-JNK (#9252), anti-p-JNK (#9106), anti-p-liver kinase B1 (LKB1) (#3482), and anti-p-calcium/calmodulin-dependent protein kinase kinase β (CaMKKβ)

(#12818) (all from Cell Signaling Technology, USA); anti-Keap1 (10503-2-AP) (Proteintech, USA); anti-NAD(P)H: quinone oxidoreductase 1 (NQO1; Ab Frontier Seoul, Korea) (ab34173); and anti-tyrosine hydroxylase (TH) (T2928) and β-actin (A-5441) (both from Sigma-Aldrich). Recombinant His-tagged Keap1 protein was obtained from Bioprogen (Korea). Biotinylated 16-mer peptide corresponding to the Nrf2 ETGE region (Biotin-AFFAQLQLDEETGEFL) was synthesized by Genscript (USA). Recombinant Keap1 Kelch domain was obtained from BPS Bioscience (USA). Vectastain ABC kit and biotinylated secondary antibodies were purchased from Vector Laboratories (USA), and the chemiluminescence detection system was procured from Pierce Chemical (USA). Chemicals used in organic compound synthesis were purchased from Acros (Belgium), Tokyo Chemical Industry (Japan), or Sigma-Aldrich. Ethyl acetate (EtOAc) and hexane were used after simple distillation with a boiling chip. All other chemicals were reagent grade and were purchased from Merck (USA) or Sigma-Aldrich.

Synthesis of KKC080096

4,6-Dichloro-2-(methylthio)pyrimidine-5-carbaldehyde (Compound 2)

Phosphoryl chloride (43.5 ml; 0.37 mol; 5.8 equivalent) was charged in a 250 ml 3-neck flask. The reaction temperature was lowered to 0°C, dimethylformamide (14 ml; 0.18 mol; 2.8 equivalent) was added dropwise, and the reaction was allowed to continue at 24°C for 1 h. 2-(Methylthio)pyrimidine-4,6-diol (10 g; 63.2 mmol) (Compound 1) was added to the reactor and heated for 24 h at 100°C. The progress of the reaction was monitored using thin layer chromatography; the R_f value (*n*-hexane/EtOAc: 10/1) of the product (ultraviolet-active) was 0.42. After completion of the reaction, the mixture was poured into ice water and was incubated for 6 h to allow the formation of a yellowish precipitate. After filtration, the filtrate was neutralized with NaHCO$_3$, and the product was extracted using EtOAc, dried over anhydrous MgSO$_4$, and evaporated. The solid crude product was dissolved in 5 ml of EtOAc and 300 ml of *n*-hexane by continuous shaking. A yellowish solid was allowed to form overnight at 4°C, which was isolated using filtration with only *n*-hexane before drying under high vacuum (0.875 g). Yield: 62%; ^{1}H NMR (400 MHz, DMSO-d_6) δ 1.54 (d, *J* = 6.5 Hz, 3H), 2.42 (s, 3H), 5.42 (s, 3H), 7.19-7.41 (m, 8H), 7.41 (d, *J* = 7.1 Hz, 2H), 8.15 (s, 1H), 8.74 (d, *J* = 7.1 Hz, 1H); ^{13}C NMR (100 MHz, DMSO-d_6) δ 14.0, 22.8, 49.6, 50.1, 98.5, 126.5, 127.2, 128.0, 128.8, 128.9, 132.8, 137.7, 145.0, 154.0, 154.9, 168.9.

1-*t*-Butyl-4-chloro-6-(methylthio)pyrazolo[3,4-d]pyrimidine (Compound 3)

Compound 2 (200 mg, 0.9 mmol) was dissolved in 20 ml tetrahydrofuran in a 50 ml 3-neck flask, and 1.5 equivalents of Hunig base were added dropwise, followed by 1.5 equivalents of *t*-butyl-N$_2$H$_3$. The reaction was allowed to continue for 24 h at 24°C. The reaction mixture was diluted with water, and the product was extracted with EtOAc, dried over anhydrous MgSO$_4$, and evaporated. The crude mixture was purified using flash chromatography with a solvent system

of n-hexane:EtOAc (8:1) to obtain a pale yellowish solid (0.2 g). Yield: 86%; ^{1}H NMR (400 MHz, DMSO-d_6) δ 1.65 (s, 9H), 2.54 (s, 3H), 8.82 (s, 1H); ^{13}C NMR (100 MHz, DMSO-d_6) δ 14.3, 29.6, 62.4, 109.7, 124.5, 155.2, 159.7, 167.8.

1-(t-Butyl)-N-(4-methoxybenzyl)-6-(methylthio)-1H-pyrazolo[3,4-d]pyrimidine-4-amine (Compound 4; KKC080096)

Compound 3 (200 mg, 0.78 mmol) was dissolved in 20 ml 1,4-dioxane in a 50 ml 3-neck flask and reacted with 4-methoxybenzylamine (118 mg, 1.1 equivalents) under reflux conditions for 8 h. After completion, the reaction mixture was diluted with water, and the product was extracted with EtOAc, dried over anhydrous MgSO$_4$, and evaporated to obtain a brown solid (0.273 g). Yield: 98%; melting point: 154.3°C; IR (KBr) ν$_{max}$ 3312, 3145, 2978, 2962, 2931, 2833, 1612, 1553, 1526, 1511, 1428, 1384, 13330, 1320, 1285, 1213, 1158, 1034, 916, 817, 777, 755, 586; ^{1}H NMR (400 MHz, CDCl$_3$) δ 1.58 (s, 9H), 2.54 (s, 3H), 3.75 (s, 3H), 4.66 (s, 2H), 6.27 (br s, 1H), 6.79 (d, J = 8.1 Hz, 2H), 7.23 (d, J = 8.4 Hz, 2H), 7.96 (s, 1H).

Cell culture

BV-2 mouse microglial cells (Blasi et al., 1990) were grown in DMEM supplemented with 10% FBS. CATH.a mouse dopaminergic neuronal cells (Suri et al., 1993) were cultured in RPMI 1640 supplemented with 8% horse serum and 4% FBS. The cells were maintained in the presence of 100 IU/l penicillin and 10 μg/ml streptomycin at 37°C in a humidified atmosphere containing 95% air and 5% CO$_2$.

Nitric oxide (NO) assay

Griess reagent (1% sulfanilamide and 0.1% naphthylethylenediamine dihydrochloride in 2.5% H$_3$PO$_4$) was combined with the cell culture medium (1:1) in a 96 well microtiter plate, and absorbance at 540 nm was read.

Reverse transcription polymerase chain reaction

The RT-PCR method, rather than quantitative real-time PCR, was used to compare mRNA levels, based on our previous finding that the results obtained from RT-PCR corresponded very well to those from real-time PCR in our experimental system (Lee et al., 2015b). First Strand cDNA Synthesis kit was employed for RT using 5 μg of total RNA as template. The following PCR cycle was employed: 94°C for 30 s, 55°C for 40 s, and 72°C for 1 min for 25 cycles using respective primers. The following gene-specific primers were used: HO-1 (forward, 5'-AGCAGGACATGGCCTCT-3'; reverse, 5'-TCTGTCAGCATCACCTGCAG-3'), interleukin-1β (IL-1β) (forward, 5'-ATGGCAACTGTTCCTGAACTCACCT-3'; reverse, 5'-CAGGACAGGTATAGATTCTTTCCTTT-3'), inducible NO synthase (iNOS) (forward, 5'-ATGTCCGAAGCAAACATCAC-3'; reverse, 5'-TAATGTCCAGGAAGTAGGTG-3'), Arg1 (forward, 5'-AGTCTGGCAGTTGGAAGC-3'; reverse, 5'-TTGGCAGATATGCAGGGAG-3'), CD206 (forward, 5'-AACAAGAATGGTGGGCAGTC-3'; reverse, 5'-CCTTTCAGTCCTTTGCAAGC-3'), YM1 (forward, 5'-GATCTCAATATACACAGTGC-3'; reverse, 5'-GAGCTTAGCCAAAGCTGAC-3'), transforming growth factor-β (TGF-β) (forward, 5'- TTGCTTCAGCTCCACAGAGA-3'; reverse, 5'-TGGTTGTAGAGGGCAAGGAC-3'), IL-10 (forward,

5'-CCAAGCCTTATCGGAAATGA-3'; reverse, 5'-TTTTCACAG-GGGAGAAATCG-3'), NQO1 (forward, 5'-CCATCCTAAACAG-CGATCA-3'; reverse, 5'-TAGCTTTGATCTGGTTGTC-3'), GCLC (forward, 5'-ATGACTGTTGCCAGTGGATGAGA-3'; reverse, 5'-ACACGCCATCCTAAACAGCGATCA-3'), GCLM (forward, 5'-AGCTGGACTCTGTGATCATGGCTT-3'; reverse, 5'-CAAAG-GCAGTCAAATCTGGTGGCA-3'), DJ-1 (forward, 5'-GCTT CCAAAAGAGCTCTGGTCA-3'; reverse, 5'-GCTCTAGTCTTT-GAGAACAAGC-3'), thioredoxin 1 (Trdx1) (forward, 5'-TACGCAATCTGAGCTGCCGAAC-3'; reverse, 5'-CTCCT-TAGCTGCTGCCAGTC-3'), catalase (forward, 5'-TGAGAAG-CCTAAGAACGCAATTC-3'; reverse, 5′-CCCTTCGCAGCCAT-GTG-3'), and glyceraldehydes-3-phosphate dehydrogenase (GAPDH; internal control) (forward, 5'-CACCACCATG-GAGAAGGCTGG-3'; reverse, 5'-TTGTCATGGATGACCTTG-GCCAGG-3'). After gel electrophoresis, the resulting bands were analyzed by densitometry using ImageJ (Schindelin et al., 2012).

Western blotting

Cell lysates and nuclear and cytosolic fractions were obtained and protein concentrations were determined for each sample. Thirty micrograms of protein were subjected to western blotting using the following primary antibodies and respective dilutions: anti-iNOS (1:200), anti-p-IKK (1:1,000), anti-IKK (1:200), anti-p-JNK (1:1,000), anti-JNK (1:1,000), anti-p-p38 (1:1,000), anti-p38 (1:1,000), anti-p-ERK (1:1,000), anti-ERK (1:1,000), anti-HO-1 (1:200), anti-p-AMPK (1:1,000), anti-AMPK (1:1,000), anti-p-LKB1 (1:1000), anti-p-CaMKKβ (1:1,000), anti-Keap1 (1:20,000), anti-Nrf2 (1:2,000), anti-GCLC (1:3,000), anti-GCLM (1:200), anti-NQO1 (1:1,000), anti-DJ-1 (1:500), lamin B (1:200), HSP90 (1:1,000), or anti-β-actin (1:60,000). After incubating with horseradish peroxidase-conjugated secondary antibodies, the resulting bands were detected using the chemiluminescence detection system.

Cell viability test

Intracellular ATP levels were measured using the CellTiter-Glo Luminescent Cell Viability Assay kit as previously reported (Woo et al., 2014).

Measurement of IL-1β levels

IL-1β levels in the lysates of BV-2 cells were measured using the ELISA kit as previously described (Son et al., 2012) and quantitated using a standard curve generated each time.

Surface plasmon resonance

The Biacore T100 instrument (GE Healthcare, Sweden) was used to perform surface plasmon resonance experiments essentially as detailed previously by us (Lee et al., 2015a). Briefly, after immobilization of anti-His antibody on CM5 chips and injecting purified His-tagged Keap1 over the immobilized anti-His antibody, KKC080096 was injected in running buffer at 30 μl/min for 180 s to allow binding to Keap1, followed by dissociation for 300 s. The sensor chip was regenerated after each cycle. The obtained sensograms were analyzed using BI-Aevaluation software (GE Healthcare). The reference surface value (running buffer only) was subtracted from the reaction

surface values to correct for non-specific interactions.

Competitive binding assay

The *in vitro* competitive binding assay was performed as per Kim et al. (2020). The biotinylated Nrf2 ETGE peptide (20 ng) was allowed to bind to streptavidin-agarose beads—in 50 mM HEPES, pH 7.6—by incubating for 1 h at 24°C. After washing, the Nrf2 peptide-conjugated beads were incubated for 5 min with recombinant Keap1-Kelch domain (50 ng) in the presence or absence of KKC080096. Next, the beads were washed, boiled in SDS-loading buffer, and subjected to western blotting using an antibody against Keap1.

HO-1 induction assay

The BV-2 cell pellet was lysed by resuspension in lysis buffer (50 μl; 150 mM NaCl, 50 mM Tris-HCl, pH 8.0 and 1% Nonidet-P40) followed by incubation on ice for 20 min. After centrifugation (3,000 × g, 15 min), the supernatant was diluted 10 fold with 50 mM Tris-HCl, pH 8.0. Sandwich ELISA for HO-1 was performed using the capture and detection HO-1 antibodies as previously detailed in our publications (Woo et al., 2014).

Generation of animals with MPTP-induced neurodegeneration

The animal study was pre-approved by the Institutional Animal Care and Use Committee at Asan Medical Center (IACUC No. 2015-13-088). Male C57BL/6 mice (23-25 g) were maintained in a temperature- and humidity-controlled facility with a 12 h light-dark cycle, and food and water were available *ad libitum*. The animals were randomly divided into three groups (n = 10 per group), control, MPTP, and MPTP+KKC080096. KKC080096 was dissolved in 10% N-methyl-2-pyrrolidone and 20% Tween 80 (pH 7.0) and administered by oral gavage three times every 24 h (30 mg/kg body weight). The control and MPTP groups received the vehicle alone. Two hours after the second KKC080096 administration, MPTP dissolved in saline was intraperitoneally injected four times at 2 h intervals (20 mg/kg body weight). The control group was injected only with saline. The animals were housed in an individually-ventilated caging system in an animal facility designated for hazardous materials handling. Motor activity tests and euthanization were performed in a separate room (one animal at a time) to minimize the emotional distress that might be experienced by the remaining live animals.

Hindlimb test

On the sixth day after MPTP injection, the mice were suspended by the tail and the posture of the hindlimb was scored (Lee et al., 2020). A score of 4 was given when both hindlimbs were splayed outward without toe clasping, which is considered a typical behavior. A score of 1 was deducted whenever there was an incomplete splay of a hindlimb (retracted toward the abdomen). Another score of 1 was deducted whenever the toes were curled (clasping) on either hindlimb.

Rotarod test

Rotarod test was performed to evaluate fore- and hindlimb motor coordination and balance. As described before (Lee et al., 2016), on days 3, 4, and 5 before MPTP injection, the mice were trained for 150 s twice a day (with a 60 min resting period between trials) on a rotarod (Ugo Basile Biological Research, Italy) that was rotating at a constant speed of 20 rpm. If the mice fell from the rod before 150 s, the animals were promptly picked up and placed on the rotarod. By the third day of training, all mice were able to stay on the rotating rod for the full 150 s. On the sixth day after the MPTP injection, the mice were tested on the rotarod rotating at a constant speed of 30 rpm, and the duration for which the mice held on to the rotarod was recorded. Three consecutive trials were performed, with a 60 min resting period between trials, and the values were averaged.

Pole test and vertical grid test

Pole test was performed as previously reported (Ogawa et al., 1985). For the vertical grid test (Kim et al., 2010), mice were trained to ascend, turn around, and descend on the vertical apparatus, twice a day on days 3, 4, and 5 before MPTP injection. On day six post-MPTP injection, the same vertical grid trials were performed and videotaped. The videos were replayed and analyzed to measure the time taken to make a turn, total time taken, and the percent of successful hindlimb steps.

Immunohistochemistry

Immunohistochemistry was performed as previously described in publications from our group (Lee et al., 2016). The animals were deeply anesthetized seven days after MPTP injection. Then, the animals were transcardially fixed in 4% paraformaldehyde, and their brains were removed. After fixation and cryoprotection, the substantia nigra (SN) and striatal tissues, identified using the mouse brain atlas (Franklin and Paxinos, 1997), were cut into 20 μm sections on a HM 450 sliding microtome (Thermo Fisher Scientific). Five sections of the SN (each 80 μm apart) were acquired, ensuring that the sections from each animal represented the same anatomical region, and were subjected to immunostaining for Iba-1 (1:200). An additional five sections of the SN—each anteriorly adjacent to those immunostained for Iba-1—were taken from each brain and subjected to TH immunostaining (1:1,000). The immunoreactivities were visualized after the sequential exposure to the Vectastain ABC kit, biotinylated secondary antibodies, and the substrate solution (0.05% 3,3'-diaminobenzidine and 0.003% H_2O_2). For quantitative analyses, the TH immunopositive neurons in the SN were counted using the Mousotron 3.8.3 program (Black Sun Software, Belgium). The TH-immunopositive fibers in the striatum and the Iba-1 immunopositive microglial cells in the SN were subjected to densitometry using the Image Gauge 4.0 program (Fujifilm, Japan). The final immunodensity values were obtained after subtracting the background density value from the regions lacking immunoreactivity. All values for each group were averaged and presented as a percentage of the vehicle-treated group ± SEM.

Data analyses

Statistical tests were performed using PRISM (GraphPad Software, USA). $P < 0.05$ was considered significant. Com-

parisons of three or more groups were analyzed by one-way ANOVA and post Dunnett's multiple comparison tests. At least three independent experiments were performed for *in vitro* studies and the data were calculated as mean ± SEM of independent experiments. For western blotting and RT-PCR, densitometric analyses were performed using ImageJ program, the data were normalized against respective loading control, and the fold increase was calculated against respective control. All western blot and RT-PCR data showed statistical significance in the above tests.

RESULTS

Identification of KKC080096 from a pyrazolo[3,4-*d*]pyrimidine library
We have a focused library consisting of 241 novel pyrazolo[3,4-*d*]pyrimidines synthesized by us. The compounds in this library were screened for their ability to upregulate HO-1, by utilizing a cell-based sandwich ELISA assay previously reported by us (Woo et al., 2014). From this screen, a novel synthetic compound 1-(*t*-butyl)-*N*-(4-methoxybenzyl)-6-(methylthio)-1*H*-pyrazolo[3,4-*d*]pyrimidine-4-amine (KKC080096) (Fig. 1A) was identified. For confirmation, we performed western blotting and RT-PCR on KKC080096-treated BV-2 murine microglial cells. The results revealed a dramatic and dose-dependent increase in HO-1 level (Fig. 1B). KKC080096 showed no cytotoxicity; cell viability did not change with

increasing concentrations of KKC080096 (Fig. 1C) ($P > 0.05$ vs untreated control). The synthesis of KKC080096 involves three steps and uses 2-(methylthio)pyrimidine-4,6-diol as the starting material (Fig. 1A). The procedure for organic synthesis is detailed in the Materials and Methods section.

KKC080096 lowers the levels of proinflammatory mediators, increases those of anti-inflammatory markers, and inhibits kinases in inflammatory signaling pathways
As HO-1 is a suppressor of inflammation, we tested whether this HO-1-activating compound might exert such effects. In LPS-challenged BV-2 cells, KKC080096 dose-dependently suppressed the generation of the inflammatory mediator NO, thereby completely abolishing the effect of LPS at 20 μM (Fig. 2A) (IC50 = 4.33 μM). The LPS-induced increase in the mRNA level of inducible NO synthase (iNOS), the enzyme responsible for NO synthesis, was also reduced by KKC080096 in a similar manner (Fig. 2C). The expression of proinflammatory cytokine IL-1β was also decreased at both protein and mRNA levels, and the LPS-induced increase in IL-1β levels was completely blocked by KKC080096 at a concentration of 20 μM (Figs. 2B and 2C) (IC50 = 4.75 μM). In comparison, while the expression of the M2-like anti-inflammatory phenotype markers Arg1, CD206, and YM1 was dramatically downregulated in LPS-stimulated cells, this was largely recovered in the background of KKC080096 treatment (Fig. 2D). Under the same conditions, the mRNA levels of the anti-inflammatory
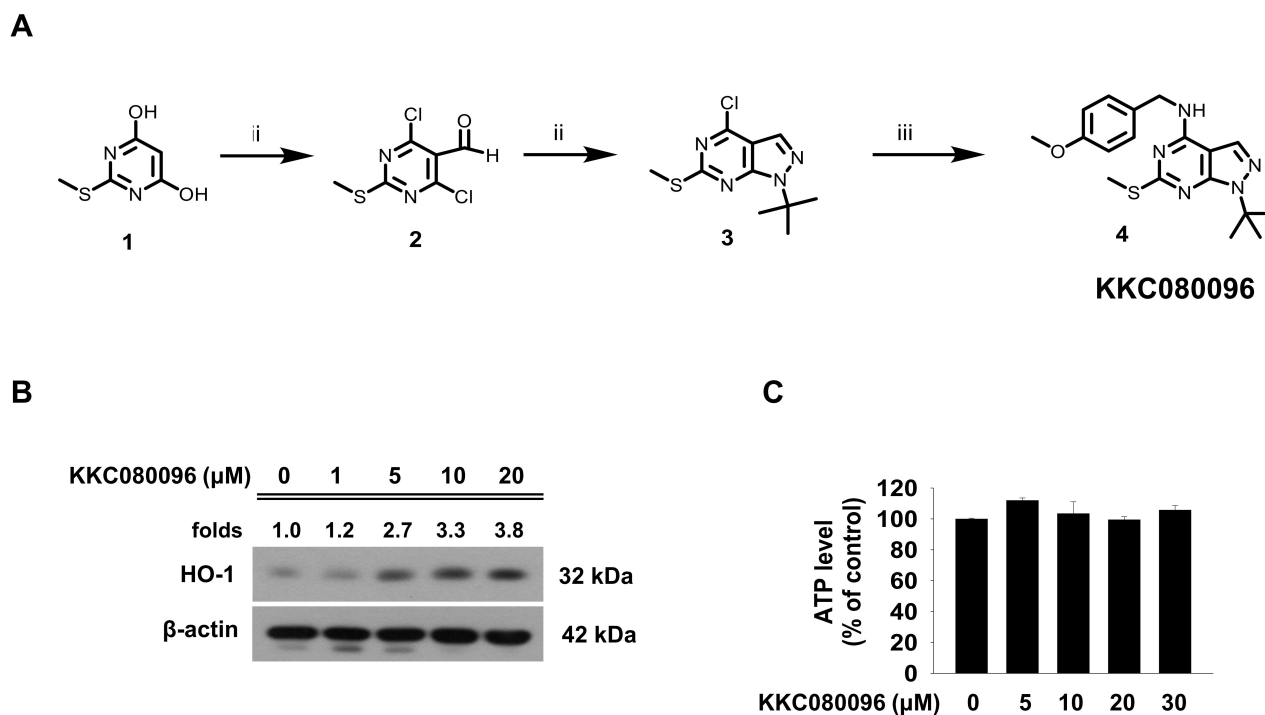
A

B

C

Fig. 1. Structure, synthesis and discovery of KKC080096 as a HO-1 inducer. (A) The synthesis scheme and chemical structure of KKC080096. (B and C) BV-2 cells were treated with various concentrations of KKC080096. (B) After 24 h, western blotting was performed for HO-1 using β-actin as a loading control. The number on each gel pictogram represents the fold increase with respect to untreated control, calculated from densitometry and normalized against respective loading control. (C) After 24 h, cell viability was assessed using the ATP assay.
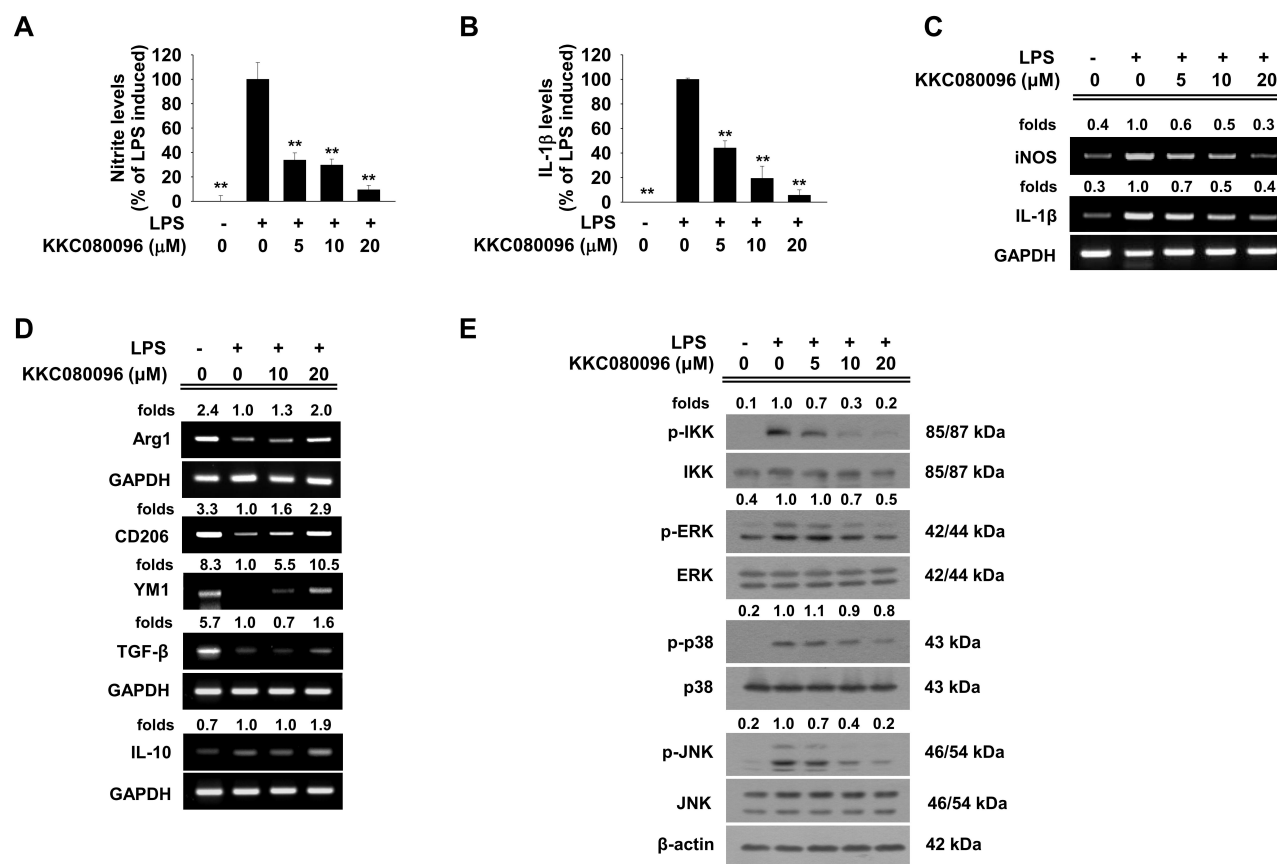
Fig. 2. KKC080096 downregulates proinflammatory gene expression, upregulates anti-inflammatory gene expression, and suppresses IKK and MAPK activation in activated microglia. BV-2 cells were stimulated with LPS (0.2 μg/ml) and treated with various concentrations of KKC080096. After 24 h, the nitrite (A) and IL-1β (B) levels were determined using the Griess assay and ELISA, respectively. The data are expressed as percentage of LPS-induced control ± SEM; **$P < 0.01$. The cells were harvested after 6 h and RT-PCR was performed for (C) iNOS and IL-1β and (D) Arg1, YM1, CD206, IL-10, and TGF-β using GAPDH as an internal control. (E) BV-2 cells were treated with various concentrations of KKC080096 for 1 h before stimulation with 0.2 μg/ml LPS. After 0.5 h, the cells were harvested, and the levels of phosphorylated and total IKK and MAPKs JNK, p38, and ERK were assessed using western blotting. (C-E) The number on each gel pictogram represents the fold change with respect to LPS-treated control, calculated from densitometry and normalized against respective internal control.

cytokines TGF-β and IL-10 were also increased (Fig. 2D).

As HO-1 interferes with IKK- and MAPK-mediated signaling, it was possible that the mechanism underlying the anti-inflammatory action of KKC080096 might involve these kinases. As shown in Fig. 2E, while LPS caused a dramatic increase in the levels of phosphorylated IKK (active form), this was dose-dependently inhibited by KKC080096; 5 μM KKC080096 lowered the phosphorylation level by 34% and 10 μM KKC080096 almost completely inhibited the phosphorylation. The effects on the MAPKs were similar; the levels of phosphorylated ERK, p38, and JNK were concomitantly increased upon LPS exposure, and this was dose-dependently suppressed by KKC080096.

KKC080096 suppresses microglial activation and provides neuroprotection in the SN of MPTP-treated mice

Based on our *in vitro* results, we investigated whether KKC080096 might also exert anti-inflammatory effects *in vivo*. We utilized the neurotoxin MPTP, whose systemic administration induces neuroinflammation and neurodegeneration in the SN (Kurkowska-Jastrz bska et al., 1999). The degree of microglial activation in the nigral region was examined by checking the expression of the microglial marker Iba-1 (Sierra et al., 2007) using immunohistochemistry. In the vehicle control animals, the Iba-1-positive cells were characterized by a ramified morphology, indicating resting microglia, whereas in MPTP-treated animals, they were characterized by an ameboid morphology, indicating activated microglia (Fig. 3A). However, the MPTP + KKC080096 animals exhibited a morphology similar to that of the control group animals. Densitometric analysis revealed that the Iba-1 immunodensity —which was increased by MPTP—was decreased by 67% by in the background of KKC080096 treatment.

Immunostaining for TH—a dopaminergic marker—revealed that while the number of surviving dopaminergic neurons in the SN was reduced by MPTP to 60%, it was significantly
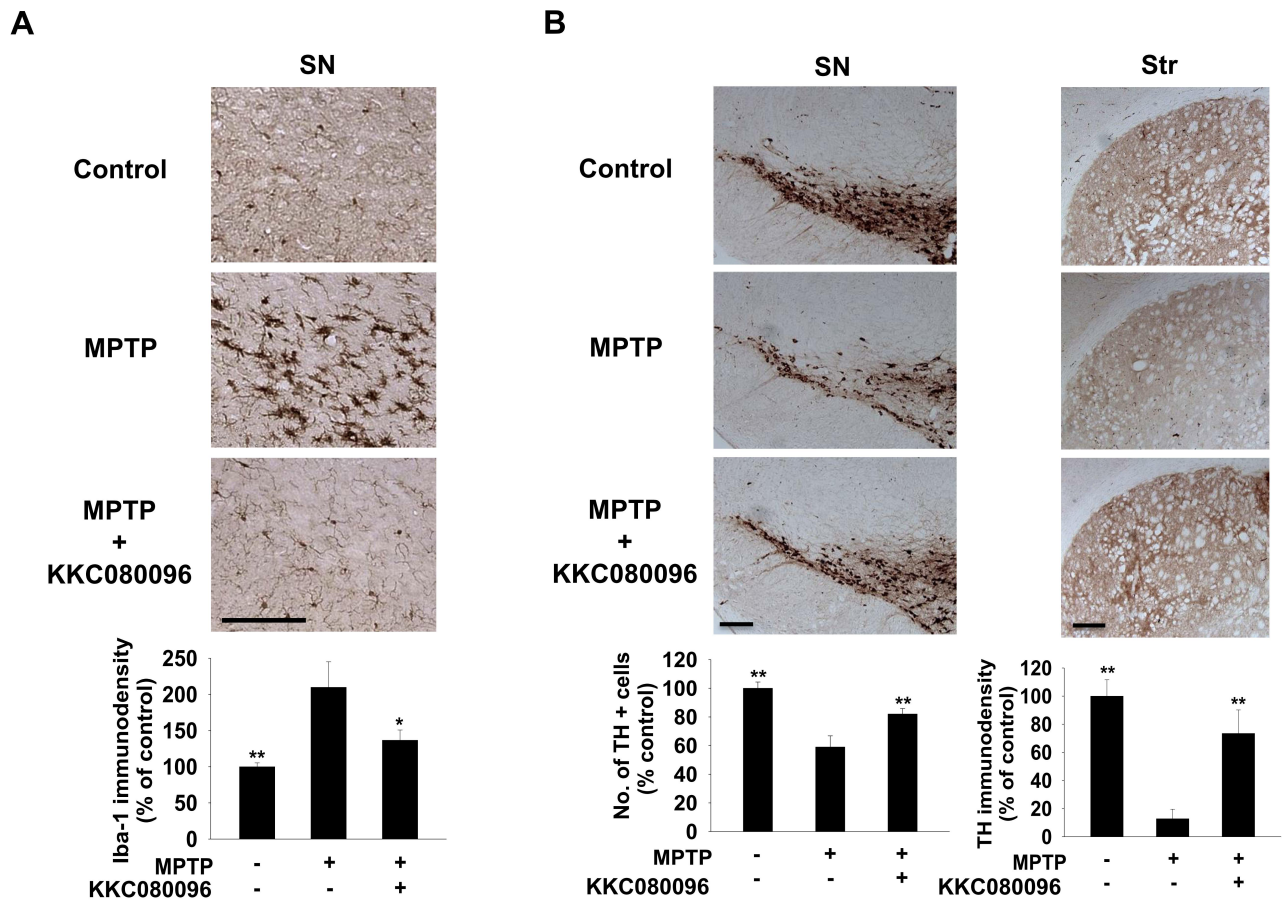
Fig. 3. KKC080096 suppresses microglial activation and protects dopaminergic neurons in MPTP-treated mice. Immunohistochemistry in mice administered MPTP alone only or co-treated with 30 mg/kg KKC080096. (A) Photomicrographs of the nigral sections showing Iba-1 expression (top) and quantitative analysis of the Iba-1-immunopositive microglia in the SN using densitometry (bottom). Scale bar = 200 μm. (B) Photomicrographs of the nigral (top left) and striatal (Str) (top right) sections immunostained against TH and quantitative analysis of the TH-immunopositive neurons in the SN by counting (bottom left) and TH-immunopositive terminals in the striatum by densitometry (bottom right). Scale bars = 200 μm. The data are expressed as the percentage of vehicle control group ± SEM; *$P < 0.05$, **$P < 0.01$ vs MPTP group.

higher in the MPTP+KKC080096 group (82%) (Fig. 3B). The effect on the fibers in the striatum, the region where the terminals of nigral dopaminergic neurons exist, was more evident: While MPTP treatment resulted in almost complete disappearance of the fibers (leaving only 13% vs untreated control), this was largely prevented by KKC080096 (74%).

KKC080096 improves motor performance of MPTP-treated mice

We investigated whether KKC080096 might also prevent the motor deficits associated with the MPTP-induced neurodegeneration by utilizing various behavioral tests shown to reliably assess the PD-associated motor deficits. On the hindlimb test, the MPTP mice scored only 32% of the vehicle control, but KKC080096 could improve this score to 75% (Fig. 4A). On the rotarod test, the MPTP + KKC080096 group could hold on for 190 s (66% of the vehicle control), while the MPTP mice could stay on the rotating rod for only 97 s (34%) (Fig. 4B). On the pole test, the reduction in the duration of

pole-hanging in the MPTP animal was completely reversed by KKC080096 (Fig. 4C, $P > 0.05$ vs vehicle control). In addition, on the vertical grid apparatus, all motor activity indices (time to make a turn on the grid, total time taken on the grid, and the number of successful hindlimb stepping; Figs. 4D-4F) were significantly improved upon KKC080096 cotreatment. Therefore, these data demonstrated that KKC080096 could protect the MPTP-treated animals from developing motor deficits typical of nigral neurodegeneration.

KKC080096 activates AMPK, LKB1, and CaMKKβ to induce HO-1 expression

Next, we sought to identify the cellular signaling involved in KKC080096-induced HO-1 expression. As HO-1 induction can be achieved via AMPK activity, we tested if KKC080096 might cause AMPK activation. When the cells were treated with KKC080096, the levels of phosphorylated AMPK (active form) were dramatically elevated, with KKC080096 causing a 2.3 fold increase at a concentration of 5 μM (Fig. 5A). AMPK
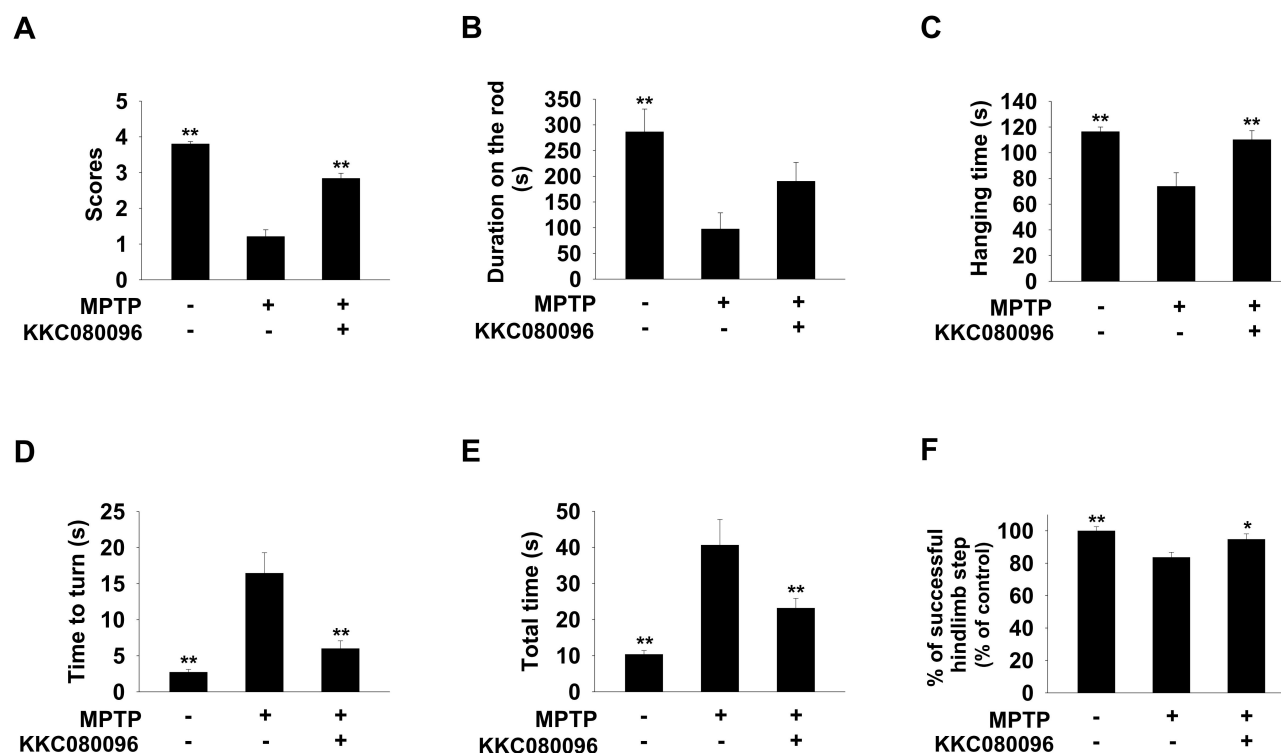
Fig. 4. KKC080096 improves motor activities in MPTP-treated mice. Motor deficit analyses of mice administered MPTP alone or co-treated with 30 mg/kg KKC080096. (A) Hindlimb test score. (B) Latent time on rotarod. (C) Hanging time on pole. (D) Time taken to make a turn on the vertical grid. (E) Total time taken on the vertical grid. (F) Percentage of successful steps made on the vertical grid. The data are expressed as mean ± SEM; *$P < 0.05$, **$P < 0.01$ vs MPTP group.

is known to be activated by the upstream kinases liver kinase B1 (LKB1) (Shaw et al., 2004; Woods et al., 2003) and calmodulin-dependent protein kinase kinase β (CaMKKβ) (Hawley et al., 2005; Woods et al., 2005). Western blotting showed that KKC080096 could increase the phosphorylation levels of both LKB1 and CaMKKβ in a manner similar to that observed with AMPK phosphorylation (Fig. 5B). Therefore, these data suggested that KKC080096 might act by activating both LKB1/AMPK and CaMKKβ/AMPK pathways to induce HO-1 expression and activity.

In order to ascertain that AMPK indeed acts upstream of HO-1 in the signaling elicited by KKC080096, we asked whether inhibition of AMPK might reverse the HO-1 induction. As shown in Fig. 5C, when the cells were pretreated with Compound C, the pharmacological inhibitor of AMPK, the KKC080096-induced HO-1 elevation was indeed diminished in a dose-dependent manner. In addition, pretreatment with this inhibitor was able to reduce the inhibitory effect of KKC080096 on the LPS-induced NO generation by 45% (Fig. 5D). The same phenomenon was noted when Ara A, another AMPK inhibitor, was tested (Fig. 5D). These data suggested that AMPK is involved in the HO-1-inducing and anti-inflammatory effects of KKC080096. Higher concentrations of these inhibitors did not have further suppressive effect (not shown), and the finding that AMPK inhibition did not completely prevent the effects of KKC080096 on HO-1 and NO

suggested involvement of additional pathway(s).

KKC080096 binds to Keap1 and competitively interferes wth Keap/Nrf2 interaction

As HO-1 expression is regulated by the transcription factor Nrf2, we tested the effect of KKC080096 on Nrf2 activation. KKC080096 increased the cellular and nuclear levels of Nrf2 protein in a dose-dependent manner (Fig. 6A). This may be due to the sequestration of Nrf2—away from its cytosolic inhibitor protein Keap1—resulting in the escape of Nrf2 from degradation (Wakabayashi et al., 2004); it was possible that KKC080096 might trigger the dissociation of Nrf2 from Keap1. We first performed surface plasmon resonance analysis to investigate if there is a physical association between KKC080096 and Keap1. For this, Keap1 protein was immobilized on a sensor chip, and the surface plasmon resonance was monitored in the presence of KKC080096. The results showed that the resonance response varied with increasing KKC080096 concentrations, demonstrating direct binding (Fig. 6B). The affinity between KKC080096 and Keap1 appeared to be quite high, as the K_d value was calculated to be 1.07E-07 M, with k_a (1/Ms) = 3.63E+05 and k_d (1/s) = 0.03874; Chi^2 (RU^2) = 1.89.

We conducted an *in vitro* competitive binding assay to observe if the binding of KKC080096 to Keap1 might actually interfere with the interaction between Nrf2 and Keap1. The
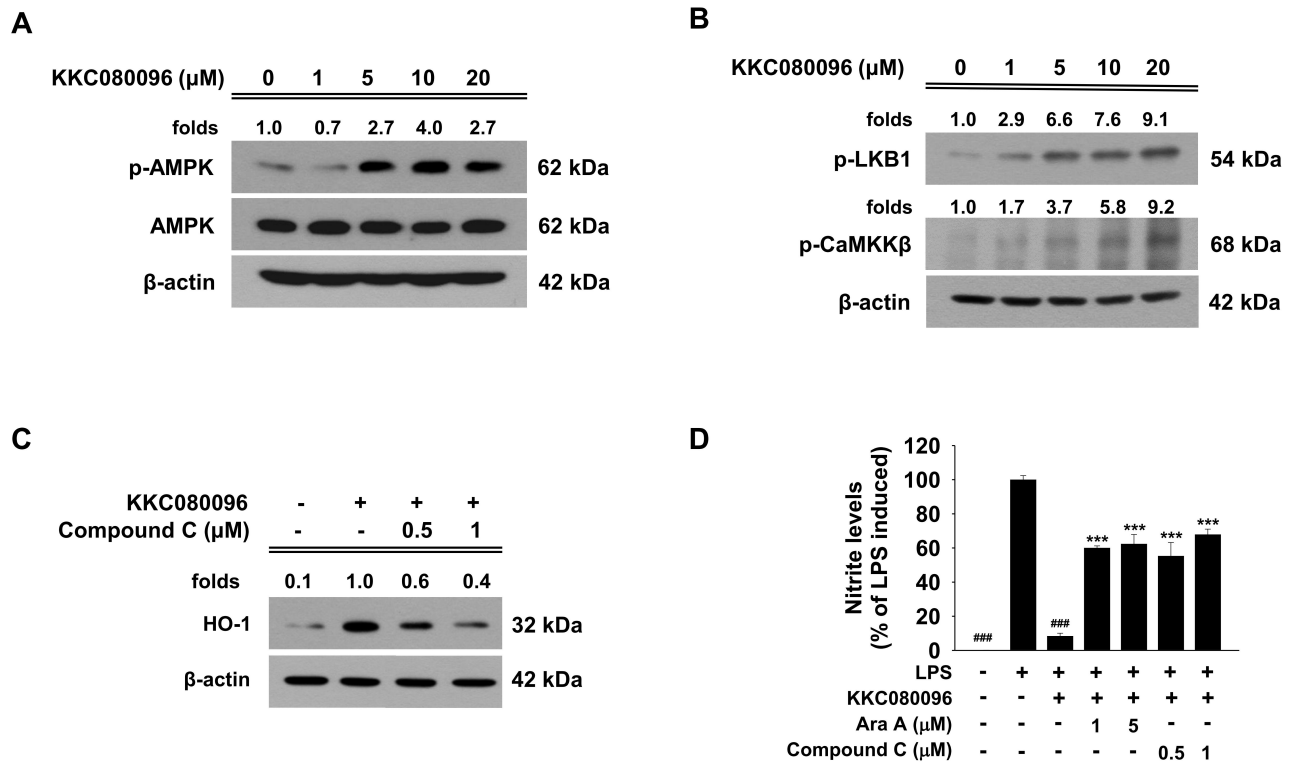
A

B

C

D

Fig. 5. KKC080096 activates AMPK, LKB1, and CaMKKβ in microglial cells. BV-2 cells were treated with various concentrations of KKC080096 for 15 min. The cells were harvested and (A) the levels of total and phosphorylated AMPK and (B) phosphorylated LKB1 and CaMKKβ were detected by western blotting with β-actin as a loading control. (C) The cells were pretreated with Compound C for 1 h, treated with KKC080096 (20 μM), and then cultured for additional 24 h. Western blotting was performed against HO-1 using β-actin as loading control. (A-C) The number on each gel pictogram represents the fold change with respect to untreated control (A and B) or KKC080096-treated control, calculated from densitometric value that had been normalized against β-actin. (D) The cells were pretreated with Ara A or Compound C for 1 h, treated with KKC080096 (20 μM) and/or 0.2 μg/ml LPS, and then cultured for additional 24 h. The nitrite level was determined using the Griess assay. The data are expressed as percentage of LPS-induced control ± SEM; [###]$P < 0.001$ vs LPS-treated; [***]$P < 0.001$ vs (KKC080096 + LPS)-treated.

Nrf2-binding Kelch domain of Keap1 and a 16-mer peptide containing the high-affinity Keap1-binding ETGE domain of Nrf2 were utilized. As shown in Fig. 6C, the presence of KKC080096 caused a decrease in the amount of Keap1 bound to Nrf2 in a dose-dependent manner, with 10 μM and 50 μM causing reductions by 28% and 64%, respectively. The data suggested that KKC080096 effectively interferes with Keap1/Nrf2 interaction.

Increased expression of the Nrf2 target genes should be another indicator of Nrf2 activation. To test this, we monitored changes in the expression of the well-known Nrf2 target genes NQO1, GCLC, and GCLM, in addition to HO-1. As shown in Fig. 6D, the mRNA levels of all three genes were indeed concomitantly and dose-dependently increased by KKC080096, providing further evidence for Nrf2 activation.

KKC080096 induces antioxidant enzyme expression in dopaminergic neuronal cells
As antioxidant enzymes exert a profound protective effect especially on dopaminergic neurons (Chang and Chen, 2020) and their expression is primarily regulated by Nrf2,

we used dopaminergic CATH.a cells to investigate whether KKC080096 can activate Nrf2 and induce the expression of antioxidant enzymes in these cells. As shown in Fig. 7A, the amount of cellular Nrf2 was indeed increased in the presence of KKC080096 in a dose-dependent manner, suggestive of sequestration from Keap1. These dopaminergic neuronal cells appeared to be much more sensitive to the compound, showing an inducing effect at concentrations as low as 0.5 μM. Therefore, we used a lower concentration range of KKC080096 in these cells. When various Nrf2 target genes were tested, the mRNA levels of all genes tested, namely HO-1, NQO1, GCLM, GCLC, DJ-1, Trdx1, and catalase, were elevated (Fig. 7B). In addition, the protein levels tested (HO-1, NQO1, GCLM, GCLC, and DJ-1) were also concomitantly elevated in a similar pattern (Fig. 7C). Thus, the Nrf2 pathway in dopaminergic neurons was also activated by KKC080096, suggesting that the increase in the expression of antioxidant enzymes might have also contributed to the neuroprotective effect of KKC080096 *in vivo*.
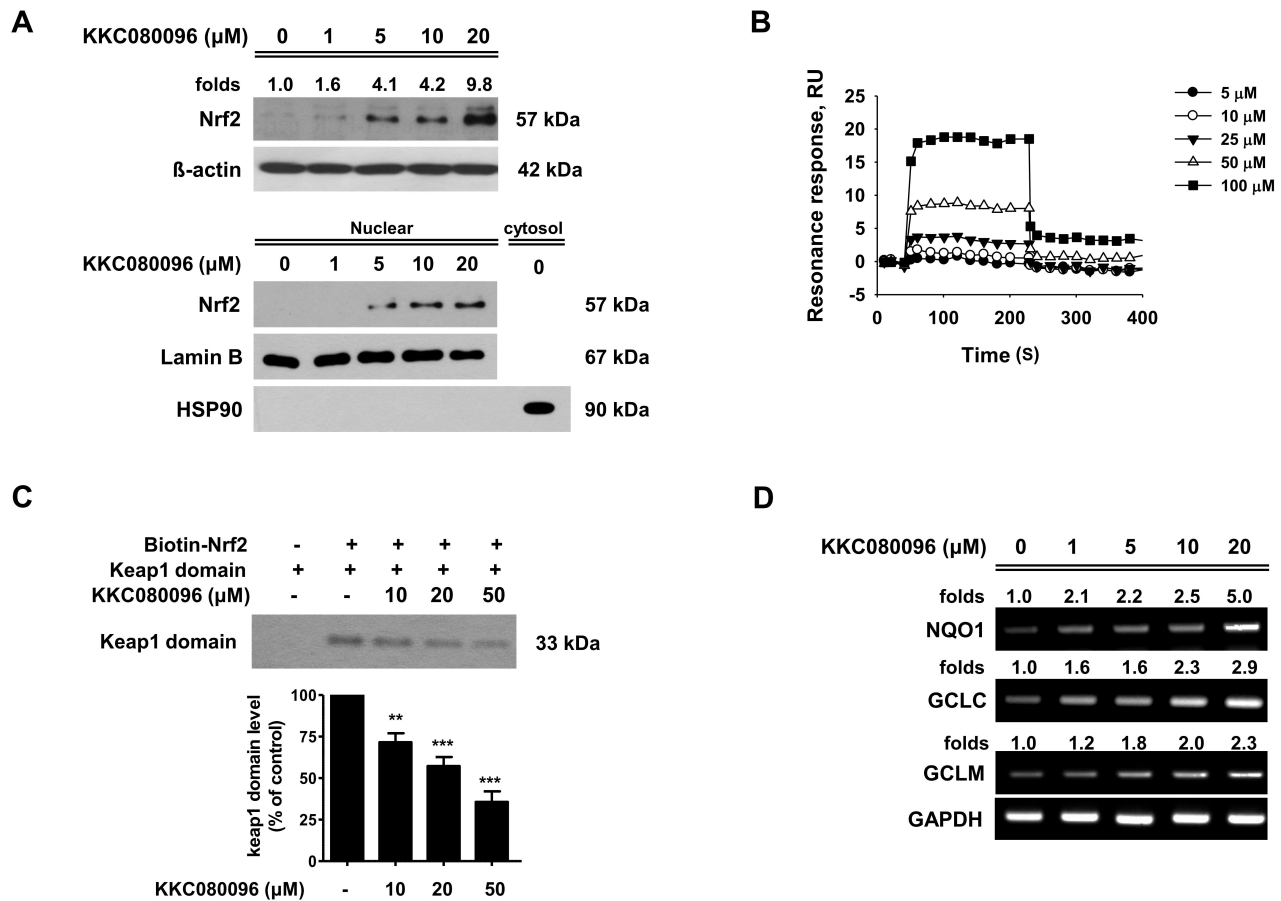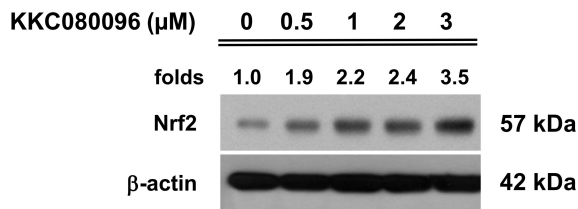
Fig. 6. KKC080096 activates Nrf2 pathway and upregulates the expression of Nrf2 target enzymes in microglial cells. (A) BV-2 cells were treated with various concentrations of KKC080096. After 24 h, the cells were harvested and the cell lysates were subjected to western blotting for Nrf2 using β-actin as an internal control (upper panel). After 6 h, the cells were harvested and the nuclear and cytosolic fractions were subjected to western blotting for Nrf2, lamin B (a nuclear marker used as an internal control), and HSP90 (a cytosolic marker used as a negative control) (lower panel). (B) Surface plasmon resonance was recorded in the presence of KKC080096. The data are expressed as resonance units (RU). (C) The biotinylated Nrf2 ETGE peptide immobilized on streptavidin-agarose beads was incubated with Keap1-Kelch domain in the presence of KKC080096, and the Nrf2-bound Keap1 was detected using western blotting. The data are plotted as percentage of control ± SEM; ∗∗$P < 0.01$, ∗∗∗$P < 0.001$. (D) BV-2 cells were treated with various concentrations of KKC080096 for 6 h. The cells were harvested and RT-PCR was performed for NQO1, GCLC, and GCLM. (A and D) The number on each gel pictogram represents the fold increase with respect to untreated control, calculated from densitometry and normalized against respective loading control.
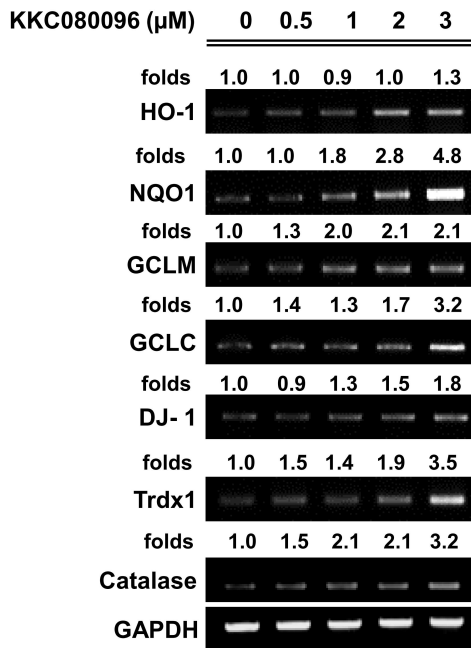
DISCUSSION

Here, we present a novel compound KKC080096 that activates the LKB1/AMPK and the CaMKKβ/AMPK pathways and Nrf2 signaling, induces HO-1 expression, and inhibits the activation of kinases involved in inflammatory signaling, ultimately resulting in the downregulation of proinflammatory mediators and upregulation of anti-inflammatory markers. The compound also induced expression of the antioxidant enzyme genes in dopaminergic neuronal cells as well as in microglia. *In vivo*, the orally administered KKC080096 could suppress neuroinflammation, protect the nigral neurons from degeneration, and alleviated the associated motor deficits in mice exposed to the dopaminergic neurotoxin MPTP.

HO-1 has been shown to act as a suppressor of inflammation. An increase in HO-1 expression has been accompanied by decreased pro-inflammatory responses in various experimental models (Cheung et al., 2009; Lin et al., 2008; Ogborne et al., 2004; Son et al., 2014), and HO-1 knockout mice exhibited chronic inflammation and enhanced vulnerability to proinflammatory endotoxins (Poss and Tonegawa, 1997; Wiesel et al., 2000). We have also shown that both gene silencing and pharmacological HO-1 inhibition abolished the anti-inflammatory effect (Lee et al., 2019). Evidence shows that HO-1 activity is involved in polarization of the microglia/macrophage toward the M2 phenotype (Naito et al., 2014; Sierra-Filardi et al., 2010; Tu et al., 2014), and this conversion reportedly prevents dopaminergic neurodegener-

A

KKC080096 (μM)	0	0.5	1	2	3	
folds	1.0	1.9	2.2	2.4	3.5	
Nrf2						57 kDa
β-actin						42 kDa

B

KKC080096 (μM)	0	0.5	1	2	3
folds	1.0	1.0	0.9	1.0	1.3
HO-1					
folds	1.0	1.0	1.8	2.8	4.8
NQO1					
folds	1.0	1.3	2.0	2.1	2.1
GCLM					
folds	1.0	1.4	1.3	1.7	3.2
GCLC					
folds	1.0	0.9	1.3	1.5	1.8
DJ- 1					
folds	1.0	1.5	1.4	1.9	3.5
Trdx1					
folds	1.0	1.5	2.1	2.1	3.2
Catalase					
GAPDH					

C

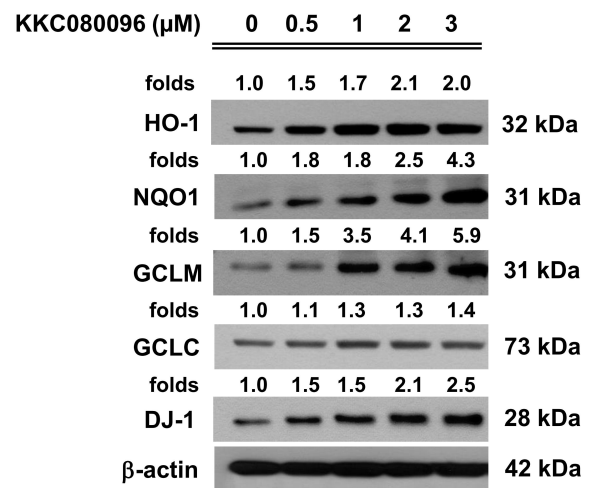| KKC080096 (μM)	0	0.5	1	2	3	
folds	1.0	1.5	1.7	2.1	2.0	
HO-1						32 kDa
folds	1.0	1.8	1.8	2.5	4.3	
NQO1						31 kDa
folds	1.0	1.5	3.5	4.1	5.9	
GCLM						31 kDa
folds	1.0	1.1	1.3	1.3	1.4	
GCLC						73 kDa
folds	1.0	1.5	1.5	2.1	2.5	
DJ-1						28 kDa
β-actin						42 kDa

Fig. 7. KKC080096 increases Nrf2 and antioxidant enzyme expression in dopaminergic neuronal cells. CATH.a cells were treated with various concentrations of KKC080096. After 24 h, cell lysate was subjected to western blotting to assess the levels of Nrf2 (A) and the antioxidant enzyme proteins (C). After 6 h, total RNA was subjected to RT-PCR to check the expression of antioxidant enzymes (B). The number on each gel pictogram represents the fold increase with respect to untreated control, calculated from densitometry and normalized against respective loading controls.

ation in the MPTP mouse PD model (Zhao et al., 2015b). We show in this study that KKC080096 caused HO-1 induction, decreased proinflammatory agent levels, increased M2 marker levels, and provided protection to the nigral dopaminergic system, all of which suggest HO-1 involvement.

HO-1 expression is induced via the Nrf2 pathway, and developing agents that target this pathway is recognized as a promising therapeutic approach for diseases involving inflammation and neurodegeneration. We show that KKC080096 binds with high affinity to Keap1, the cytosolic inhibitor of Nrf2, interferes with the Keap1-Nrf2 interaction, and leads to an increase in cellular Nrf2 level and induction of Nrf2 target genes, all of which demonstrate activation of the Nrf2 pathway. The existing Nrf2-activators like sulforaphane and bardoxolone-methyl (CDDO)-Me have been shown to cause adverse side effects in clinical studies (Baier et al., 2014; de Zeeuw et al., 2013), presumably because they are electrophil-

ic in nature and can covalently and non-specifically modify sulfhydryl groups in cellular proteins and reduced glutathione (Satoh and Lipton, 2017). However, KKC080096 possesses no electrophilic group, suggesting that its interaction with Keap1 is most likely non-covalent. Because it has a flat ring structure, the interaction may occur via pi-pi stacking, which involves non-covalent attraction between two molecules that possess flat ring structures and is known to contribute to high affinity binding pivotal to protein-ligand recognition (Zhao et al., 2015a). Based on our finding that KKC080096 disrupted the interaction between the Kelch domain of Keap1 and Nrf2, it is likely that the KKC080096-binding region lies in this domain. Since it is known that the Phe577, Tyr334, and Tyr 572 aromatic rings residing in the Kelch domain can interact with many small molecules (Schmoll et al., 2017), one of these may be the site of the pi-pi stacking with KKC080096. This notion is supported by our previous finding that another

pyrazolo[3,4-*d*]pyrimidine compound KKC080106 [(R)-1-benzyl-6-(methylthio)-*N*-(1-phenylethyl)-1*H*-pyrazolo[3,4-*d*]pyrimidine-4-amine] also binds Keap1 with high affinity (Lee et al., 2020). Further studies utilizing molecular docking simulation should be able to more closely predict the binding mode of KKC080096 to Keap1.

HO-1 expression can also be induced via AMPK (Al-Rashed et al., 2018; Thornton et al., 2016). The anti-inflammatory role of AMPK has been recognized, as its activation inhibited LPS-induced inflammatory response in glial cells (Giri et al., 2004) and suppressed the pro-inflammatory NFkB and MAPKs pathways (Ewart et al., 2008; Hattori et al., 2006; Sag et al., 2008; Salminen et al., 2011), whereas AMPK-deficiency abolished the anti-inflammatory effect of metformin (Huang et al., 2009), causing greater inflammation in mice (Galic et al., 2011) and amplifying proinflammatory signaling (Carroll et al., 2013). We show that KKC080096 activates the two upstream AMPK activators: LKB1 and CaMKKβ. The LKB1/AMPK signaling pathway has been shown to inhibit the NLRP3 inflammasome (Liu et al., 2019), suppress LPS-induced NFkB activation (Liu et al., 2015), and lead to M1 to M2 phenotype conversion (Ji et al., 2018). In addition, the CaMKKβ/AMPK pathway can reduce microglia activation by promoting microglial M2 polarization (Li et al., 2018; Xu et al., 2015; Zhou et al., 2014), and inhibit the LPS-activated NFκB signaling (Kanno et al., 2016).

It has been reported that a crosstalk exists between Nrf2 and AMPK signaling (Mo et al., 2014; Zimmermann et al., 2015), and phosphorylation of Nrf2 by AMPK facilitates its nuclear accumulation (Joo et al., 2016) and transactivates a subset of Nrf2 target genes including HO-1 (Matzinger et al., 2020). Therefore, in addition to the canonical activation involving the sequestration of Nrf2 from Keap1, KKC080096 can further facilitate Nrf2 signaling by activating AMPK. Furthermore, we have previously shown that HO-1 expression can also be induced by AMPK independent of Nrf2 (Lee et al., 2018). Therefore, the dual activity of KKC080096, i.e., activation of both AMPK/HO-1 and Nrf2/HO-1 pathways, makes this compound a valuable agent as an anti-inflammatory and neuroprotective therapy.

The IC50 of KKC080096 for NO and IL-1β were found to be in the micromolar range (4.33 μM and 4.75 μM, respectively), based on the data obtained from cell-based assay. However, its K_d value for Keap1, as determined from surface plasmon resonance study, was lower (0.1 μM). It is possible to speculate that this discrepancy is due to somewhat low efficiency of KKC080096 in traversing the plasma membrane before reaching the cytosolic protein Keap1. Modification of the compound for better membrane permeability may enhance the compound's efficacy in the cell system.

In conclusion, our novel compound KKC080096 exhibits anti-inflammatory activity, and this appears to involve the dual activation of AMPK/HO-1 and Nrf2/HO-1 signaling. *In vivo*, KKC080096 exerts anti-inflammatory effects and protects nigral neurons from degeneration, and this was accompanied by alleviation of the associated motor deficits. Thus, this novel pyrazolo[3,4-*d*]pyrimidine may be of important translational value as a therapy against neurodegenerative diseases such as PD.

AUTHOR CONTRIBUTIONS

O.H. and D.J.K. conceptualized and designed the study. J.A.L., H.R.K., N.S., H.J.S., and Y.W.K. performed the experiments. D.J.K. and C.S.C. designed and carried out organic syntheses. O.H. and J.A.L. analyzed the data and wrote the manuscript.

CONFLICT OF INTEREST

The authors have no potential conflicts of interest to disclose.

ORCID

Ji Ae Lee	https://orcid.org/0000-0003-2194-3000
Young-Won Kwon	https://orcid.org/0000-0002-7017-1126
Hye Ri Kim	https://orcid.org/0000-0002-8903-5263
Nari Shin	https://orcid.org/0000-0002-1944-4117
Hyo Jin Son	https://orcid.org/0000-0002-9264-107X
Chan Seong Cheong	https://orcid.org/0000-0002-6872-107X
Dong Jin Kim	https://orcid.org/0000-0001-8149-8610
Onyou Hwang	https://orcid.org/0000-0003-4699-9596

REFERENCES

Alam, J., Stewart, D., Touchard, C., Boinapally, S., Choi, A.M., and Cook, J.L. (1999). Nrf2, a Cap'n'Collar transcription factor, regulates induction of the heme oxygenase-1 gene. J. Biol. Chem. *274*, 26071-26078.

Al-Rashed, F., Calay, D., Lang, M., Thornton, C.C., Bauer, A., Kiprianos, A., Haskard, D.O., Seneviratne, A., Boyle, J.J., Schönthal, A.H., et al. (2018). Celecoxib exerts protective effects in the vascular endothelium via COX-2-independent activation of AMPK-CREB-Nrf2 signalling. Sci. Rep. *8*, 6271.

Arthur, J.S. and Ley, S.C. (2013). Mitogen-activated protein kinases in innate immunity. Nat. Rev. Immunol. *13*, 679-692.

Baier, S.R., Zbasnik, R., Schlegel, V., and Zempleni, J. (2014). Off-target effects of sulforaphane include the derepression of long terminal repeats through histone acetylation events. J. Nutr. Biochem. *25*, 665-668.

Blasi, E., Barluzzi, R., Bocchini, V., Mazzolla, R., and Bistoni, F. (1990). Immortalization of murine microglial cells by a v-raf/v-myc carrying retrovirus. J. Neuroimmunol. *27*, 229-237.

Carroll, K.C., Viollet, B., and Suttles, J. (2013). AMPKα1 deficiency amplifies proinflammatory myeloid APC activity and CD40 signaling. J. Leukoc. Biol. *94*, 1113-1121.

Chang, K.H. and Chen, C.M. (2020). The role of oxidative stress in Parkinson's disease. Antioxidants (Basel) *9*, 597.

Chauhan, M. and Kumar, R. (2013). Medicinal attributes of pyrazolo[3,4-d] pyrimidines: a review. Bioorg. Med. Chem. *21*, 5657-5668.

Cheung, K.L., Khor, T.O., and Kong, A.N. (2009). Synergistic effect of combination of phenethyl isothiocyanate and sulforaphane or curcumin and sulforaphane in the inhibition of inflammation. Pharm. Res. *26*, 224-231.

de Zeeuw, D., Akizawa, T., Audhya, P., Bakris, G.L., Chin, M., Christ-Schmidt, H., Goldsberry, A., Houser, M., Krauth, M., Lambers Heerspink, H.J., et al. (2013). Bardoxolone methyl in type 2 diabetes and stage 4 chronic kidney disease. N. Engl. J. Med. *369*, 2492-2503.

Ewart, M.A., Kohlhaas, C.F., and Salt, I.P. (2008). Inhibition of tumor necrosis factor α-stimulated monocyte adhesion to human aortic endothelial cells by AMP-activated protein kinase. Arterioscler. Thromb. Vasc. Biol. *28*, 2255-2257.

Franklin, K.B.J. and Paxinos, G. (1997). The Mouse Brain in Stereotaxic Coordinates (San Diego: Academic Press).

Galic, S., Fullerton, M.D., Schertzer, J.D., Sikkema, S., Marcinko, K., Walkley, C.R., Izon, D., Honeyman, J., Chen, Z.P., van Denderen, B.J., et al. (2011). Hematopoietic AMPKβ1 reduces mouse adipose tissue macrophage inflammation and insulin resistance in obesity. J. Clin. Invest. *121*, 4903-4915.

Giri, S., Nath, N., Smith, B., Viollet, B., Singh, A.K., and Singh, I. (2004). 5-aminoimidazole-4-carboxamide-1-β-4-ribofuranoside inhibits proinflammatory response in glial cells: a possible role of AMP-activated protein kinase. J. Neurosci. *24*, 479-487.

Hattori, Y., Suzuki, K., Hattori, S., and Kasai, K. (2006). Metformin inhibits cytokine-induced nuclear factor kappaB activation via AMP-activated protein kinase activation in vascular endothelial cells. Hypertension *47*, 1183-1188.

Hawley, S.A., Pan, D.A., Mustard, K.J., Ross, L., Bain, J., Edelman, A.M., Frenguelli, B.G., and Hardie, D.G. (2005). Calmodulin-dependent protein kinase kinase-β is an alternative upstream kinase for AMP-activated protein kinase. Cell Metab. *2*, 9-19.

Huang, N.L., Chiang, S.H., Hsueh, C.H., Liang, Y.J., Chen, Y.J., and Lai, L.P. (2009). Metformin inhibits TNF-α-induced IκB kinase phosphorylation, IκB-α degradation and IL-6 production in endothelial cells through PI3K-dependent AMPK phosphorylation. Int. J. Cardiol. *134*, 169-175.

Ji, J., Xue, T.F., Guo, X.D., Yang, J., Guo, R.B., Wang, J., Huang, J.Y., Zhao, X.J., and Sun, X.L. (2018). Antagonizing peroxisome proliferator-activated receptor gamma facilitates M1-to-M2 shift of microglia by enhancing autophagy via the LKB1-AMPK signaling pathway. Aging Cell *17*, e12774.

Joo, M.S., Kim, W.D., Lee, K.Y., Kim, J.H., Koo, J.H., and Kim, S.G. (2016). AMPK facilitates nuclear accumulation of Nrf2 by phosphorylating at serine 550. Mol. Cell. Biol. *36*, 1931-1942.

Kanno, Y., Ishisaki, A., Kawashita, E., Kuretake, H., Ikeda, K., and Matsuo, O. (2016). uPA attenuated LPS-induced inflammatory osteoclastogenesis through the plasmin/PAR-1/Ca2+/CaMKK/AMPK axis. Int. J. Biol. Sci. *12*, 63-71.

Kawai, T. and Akira, S. (2007). Signaling to NF-κB by Toll-like receptors. Trends Mol. Med. *13*, 460-469.

Kim, S., Indu Viswanath, A.N., Park, J.H., Lee, H.E., Park, A.Y., Choi, J.W., Kim, H.J., Londhe, A.M., Jang, B.K., Lee, J., et al. (2020). Nrf2 activator via interference of Nrf2-Keap1 interaction has antioxidant and anti-inflammatory properties in Parkinson's disease animal model. Neuropharmacology *167*, 107989.

Kim, S.T., Son, H.J., Choi, J.H., Ji, I.J., and Hwang, O. (2010). Vertical grid test and modified horizontal grid test are sensitive methods for evaluating motor dysfunctions in the MPTP mouse model of Parkinson's disease. Brain Res. *1306*, 176-183.

Kurkowska-Jastrzębska, I., Wrońska, A., Kohutnicka, M., Czlonkowski, A., and Czlonkowska, A. (1999). The inflammatory reaction following 1-methyl-4-phenyl-1,2,3, 6-tetrahydropyridine intoxication in mouse. Exp. Neurol. *156*, 50-61.

Lee, E., Eo, J.C., Lee, C., and Yu, J.W. (2021). Distinct features of brain-resident macrophages: microglia and non-parenchymal brain macrophages. Mol. Cells *44*, 281-291.

Lee, J.A., Kim, D.J., and Hwang, O. (2019). KMS99220 exerts anti-inflammatory effects, activates the Nrf2 signaling and interferes with IKK, JNK and p38 MAPK via HO-1. Mol. Cells *42*, 702-710.

Lee, J.A., Kim, H.R., Kim, J., Park, K.D., Kim, D.J., and Hwang, O. (2018). The novel neuroprotective compound KMS99220 has an early anti-neuroinflammatory effect via AMPK and HO-1, independent of Nrf2. Exp. Neurobiol. *27*, 408-418.

Lee, J.A., Kim, H.R., Son, H.J., Shin, N., Han, S.H., Cheong, C.S., Kim, D.J., and Hwang, O. (2020). A novel pyrazolo [3,4-d] pyrimidine, KKC080106, activates the Nrf2 pathway and protects nigral dopaminergic neurons.

Exp. Neurol. *332*, 113387.

Lee, J.A., Kim, J.H., Woo, S.Y., Son, H.J., Han, S.H., Jang, B.K., Choi, J.W., Kim, D.J., Park, K.D., and Hwang, O. (2015b). A novel compound VSC2 has anti-inflammatory and antioxidant properties in microglia and in Parkinson's disease animal model. Br. J. Pharmacol. *172*, 1087-1100.

Lee, J.A., Son, H.J., Kim, J.H., Park, K.D., Shin, N., Kim, H.R., Kim, E.M., Kim, D.J., and Hwang, O. (2016). A novel synthetic isothiocyanate ITC-57 displays antioxidant, anti-inflammatory, and neuroprotective properties in a mouse Parkinson's disease model. Free Radic. Res. *50*, 1188-1199.

Lee, J.A., Son, H.J., Park, K.D., Han, S.H., Shin, N., Kim, J.H., Kim, H.R., Kim, D.J., and Hwang, O. (2015a). A novel compound ITC-3 activates the Nrf2 signaling and provides neuroprotection in Parkinson's disease models. Neurotox. Res. *28*, 332-345.

Li, C., Zhang, C., Zhou, H., Feng, Y., Tang, F., Hoi, M.P.M., He, C., Ma, D., Zhao, C., and Lee, S.M.Y. (2018). Inhibitory effects of betulinic acid on LPS-induced neuroinflammation involve M2 microglial polarization via CaMKKβ-dependent AMPK activation. Front. Mol. Neurosci. *11*, 98.

Li, W., Khor, T.O., Xu, C., Shen, G., Jeong, W.S., Yu, S., and Kong, A.N. (2008). Activation of Nrf2-antioxidant signaling attenuates NFκB-inflammatory response and elicits apoptosis. Biochem. Pharmacol. *76*, 1485-1489.

Lin, W., Wu, R.T., Wu, T., Khor, T.O., Wang, H., and Kong, A.N. (2008). Sulforaphane suppressed LPS-induced inflammation in mouse peritoneal macrophages through Nrf2 dependent pathway. Biochem. Pharmacol. *76*, 967-973.

Liu, W., Bai, F., Wang, H., Liang, Y., Du, X., Liu, C., Cai, D., Peng, J., Zhong, G., Liang, X., et al. (2019). Tim-4 inhibits NLRP3 inflammasome via the LKB1/AMPKαvz pathway in macrophages. J. Immunol. *203*, 990-1000.

Liu, Z., Zhang, W., Zhang, M., Zhu, H., Moriasi, C., and Zou, M.H. (2015). Liver kinase B1 suppresses lipopolysaccharide-induced nuclear factor κB (NF-κB) activation in macrophages. J. Biol. Chem. *290*, 2312-2320.

Matzinger, M., Fischhuber, K., Pölöske, D., Mechtler, K., and Heiss, E.H. (2020). AMPK leads to phosphorylation of the transcription factor Nrf2, tuning transactivation of selected target genes. Redox Biol. *29*, 101393.

Mo, C., Wang, L., Zhang, J., Numazawa, S., Tang, H., Tang, X., Han, X., Li, J., Yang, M., Wang, Z., et al. (2014). The crosstalk between Nrf2 and AMPK signal pathways is important for the anti-inflammatory effect of berberine in LPS-stimulated macrophages and endotoxin-shocked mice. Antioxid. Redox Signal. *20*, 574-588.

Morse, D., Pischke, S.E., Zhou, Z., Davis, R.J., Flavell, R.A., Loop, T., Otterbein, S.L., Otterbein, L.E., and Choi, A.M. (2003). Suppression of inflammatory cytokine production by carbon monoxide involves the JNK pathway and AP-1. J. Biol. Chem. *278*, 36993-36998.

Naito, Y., Takagi, T., and Higashimura, Y. (2014). Heme oxygenase-1 and anti-inflammatory M2 macrophages. Arch. Biochem. Biophys. *564*, 83-88.

Ogawa, N., Hirose, Y., Ohara, S., Ono, T., and Watanabe, Y. (1985). A simple quantitative bradykinesia test in MPTP-treated mice. Res. Commun. Chem. Pathol. Pharmacol. *50*, 435-441.

Ogborne, R.M., Rushworth, S.A., Charalambos, C.A., and O'Connell, M.A. (2004). Haem oxygenase-1: a target for dietary antioxidants. Biochem. Soc. Trans. *32*, 1003-1005.

Poss, K.D. and Tonegawa, S. (1997). Heme oxygenase 1 is required for mammalian iron reutilization. Proc. Natl. Acad. Sci. U. S. A. *94*, 10919-10924.

Rojo, A.I., McBean, G., Cindric, M., Egea, J., López, M.G., Rada, P., Zarkovic, N., and Cuadrado, A. (2014). Redox control of microglial function: molecular mechanisms and functional significance. Antioxid. Redox Signal. *21*, 1766-1801.

Sag, D., Carling, D., Stout, R.D., and Suttles, J. (2008). Adenosine 5'-monophosphate-activated protein kinase promotes macrophage polarization to an anti-inflammatory functional phenotype. J. Immunol. *181*, 8633-8641.

Salminen, A., Hyttinen, J.M., and Kaarniranta, K. (2011). AMP-activated protein kinase inhibits NF-κB signaling and inflammation: impact on healthspan and lifespan. J. Mol. Med. (Berl.) *89*, 667-676.

Satoh, T. and Lipton, S. (2017). Recent advances in understanding NRF2 as a druggable target: development of pro-electrophilic and non-covalent NRF2 activators to overcome systemic side effects of electrophilic drugs like dimethyl fumarate. F1000Res. *6*, 2138.

Schindelin, J., Arganda-Carreras, I., Frise, E., Kaynig, V., Longair, M., Pietzsch, T., Preibisch, S., Rueden, C., Saalfeld, S., Schmid, B., et al. (2012). Fiji: an open-source platform for biological-image analysis. Nat. Methods *9*, 676-682.

Schmoll, D., Engel, C.K., and Glombik, H. (2017). The Keap1-Nrf2 protein-protein interaction: a suitable target for small molecules. Drug Discov. Today Technol. *24*, 11-17.

Shaw, R.J., Kosmatka, M., Bardeesy, N., Hurley, R.L., Witters, L.A., DePinho, R.A., and Cantley, L.C. (2004). The tumor suppressor LKB1 kinase directly activates AMP-activated kinase and regulates apoptosis in response to energy stress. Proc. Natl. Acad. Sci. U. S. A. *101*, 3329-3335.

Sierra, A., Gottfried-Blackmore, A.C., McEwen, B.S., and Bulloch, K. (2007). Microglia derived from aging mice exhibit an altered inflammatory profile. Glia *55*, 412-424.

Sierra-Filardi, E., Vega, M.A., Sánchez-Mateos, P., Corbí, A.L., and Puig-Kröger, A. (2010). Heme oxygenase-1 expression in M-CSF-polarized M2 macrophages contributes to LPS-induced IL-10 release. Immunobiology *215*, 788-795.

Silva, G., Cunha, A., Grégoire, I.P., Seldon, M.P., and Soares, M.P. (2006). The antiapoptotic effect of heme oxygenase-1 in endothelial cells involves the degradation of p38 α MAPK isoform. J. Immunol. *177*, 1894-1903.

Son, H.J., Lee, J.A., Shin, N., Choi, J.H., Seo, J.W., Chi, D.Y., Lee, C.S., Kim, E.M., Choe, H., and Hwang, O. (2012). A novel compound PTIQ protects the nigral dopaminergic neurones in an animal model of Parkinson's disease induced by MPTP. Br. J. Pharmacol. *165*, 2213-2227.

Son, Y., Chung, H.T., and Pae, H.O. (2014). Differential effects of resveratrol and its natural analogs, piceatannol and 3,5,4'-trans-trimethoxystilbene, on anti-inflammatory heme oxigenase-1 expression in RAW264.7 macrophages. Biofactors *40*, 138-145.

Suri, C., Fung, B.P., Tischler, A.S., and Chikaraishi, D.M. (1993). Catecholaminergic cell lines from the brain and adrenal glands of tyrosine hydroxylase-SV40 T antigen transgenic mice. J. Neurosci. *13*, 1280-1291.

Thornton, C.C., Al-Rashed, F., Calay, D., Birdsey, G.M., Bauer, A., Mylroie, H., Morley, B.J., Randi, A.M., Haskard, D.O., Boyle, J.J., et al. (2016). Methotrexate-mediated activation of an AMPK-CREB-dependent pathway: a novel mechanism for vascular protection in chronic systemic inflammation. Ann. Rheum. Dis. *75*, 439-448.

Tu, T.H., Joe, Y., Choi, H.S., Chung, H.T., and Yu, R. (2014). Induction of heme oxygenase-1 with hemin reduces obesity-induced adipose tissue inflammation via adipose macrophage phenotype switching. Mediators Inflamm. *2014*, 290708.

Wakabayashi, N., Dinkova-Kostova, A.T., Holtzclaw, W.D., Kang, M.I., Kobayashi, A., Yamamoto, M., Kensler, T.W., and Talalay, P. (2004). Protection against electrophile and oxidant stress by induction of the phase 2 response: fate of cysteines of the Keap1 sensor modified by inducers. Proc. Natl. Acad. Sci. U. S. A. *101*, 2040-2045.

Wiesel, P., Patel, A.P., DiFonzo, N., Marria, P.B., Sim, C.U., Pellacani, A., Maemura, K., LeBlanc, B.W., Marino, K., Doerschuk, C.M., et al. (2000). Endotoxin-induced mortality is related to increased oxidative stress and end-organ dysfunction, not refractory hypotension, in heme oxygenase-1-deficient mice. Circulation *102*, 3015-3022.

Woo, S.Y., Kim, J.H., Moon, M.K., Han, S.H., Yeon, S.K., Choi, J.W., Jang, B.K., Song, H.J., Kang, Y.G., Kim, J.W., et al. (2014). Discovery of vinyl sulfones as a novel class of neuroprotective agents toward Parkinson's disease therapy. J. Med. Chem. *57*, 1473-1487.

Woods, A., Dickerson, K., Heath, R., Hong, S.P., Momcilovic, M., Johnstone, S.R., Carlson, M., and Carling, D. (2005). Ca2+/calmodulin-dependent protein kinase kinase-β acts upstream of AMP-activated protein kinase in mammalian cells. Cell Metab. *2*, 21-33.

Woods, A., Johnstone, S.R., Dickerson, K., Leiper, F.C., Fryer, L.G., Neumann, D., Schlattner, U., Wallimann, T., Carlson, M., and Carling, D. (2003). LKB1 is the upstream kinase in the AMP-activated protein kinase cascade. Curr. Biol. *13*, 2004-2008.

Xu, Y., Xu, Y., Wang, Y., Wang, Y., He, L., Jiang, Z., Huang, Z., Liao, H., Li, J., Saavedra, J.M., et al. (2015). Telmisartan prevention of LPS-induced microglia activation involves M2 microglia polarization via CaMKKβ-dependent AMPK activation. Brain Behav. Immun. *50*, 298-313.

Zhao, Y., Li, J., Gu, H., Wei, D., Xu, Y.C., Fu, W., and Yu, Z. (2015a). Conformational preferences of π–π stacking between ligand and protein, analysis derived from crystal structure data geometric preference of π–π interaction. Interdiscip. Sci. *7*, 211-220.

Zhao, Y.F., Zhang, Q., Xi, J.Y., Li, Y.H., Ma, C.G., and Xiao, B.G. (2015b). Multitarget intervention of Fasudil in the neuroprotection of dopaminergic neurons in MPTP-mouse model of Parkinson's disease. J. Neurol. Sci. *353*, 28-37.

Zhou, X., Cao, Y., Ao, G., Hu, L., Liu, H., Wu, J., Wang, X., Jin, M., Zheng, S., Zhen, X., et al. (2014). CaMKKβ-dependent activation of AMP-activated protein kinase is critical to suppressive effects of hydrogen sulfide on neuroinflammation. Antioxid. Redox Signal. *21*, 1741-1758.

Zimmermann, K., Baldinger, J., Mayerhofer, B., Atanasov, A.G., Dirsch, V.M., and Heiss, E.H. (2015). Activated AMPK boosts the Nrf2/HO-1 signaling axis—a role for the unfolded protein response. Free Radic. Biol. Med. *88*(Pt B), 417-426.